Detection of crustal movements due to the 11 April 2011 Fukushima earthquake from SAR images

Wen Liu[1], Fumio Yamazaki[2], Masashi Matsuoka[1], Takashi Nonaka[3], Tadashi Sasagawa[3]
[1] Interdisciplinary Graduate School of Science and Engineering, Tokyo Institute of Technology
4259 Nagatsuta, Midori-ku, Yokohama, Japan, w.alice.liu@gmail.com; matsuoka.m.ab@m.titech.ac.jp
[2] Graduate School of Engineering, Chiba University
1-33 Yayoi-cho, Inage-ku, Chiba, Japan, fumio.yamazaki@faculty.chiba-u.jp
[3] Satellite Business Division, PASCO Corporation
4-10-1 Nakano, Nakano-Ku, Tokyo, Japan, taakka9299@pasco.co.jp; taawda5004@pasco.co.jp

Abstract – The Fukushima Earthquake with Mw7.1 occurred on April 11, 2011 was one of the most damaging induced events of the 2011 Tohoku earthquake with Mw9.0. It caused numerous fault scarps with a maximum displacement of 2.3 m. In this study, two methods were used to detect crustal movements from two different types of SAR images. Firstly, a differential interferometric analysis (DInSAR) was applied to pre- and post-event ALOS/PALSAR data. From the result of DInSAR, the trends of crustal movements in different areas could be grasped. Then an improved pixel-offset method was applied to pre- and post-event TerraSAR-X images. The two-dimensional movements were detected from the displacements of no-changed buildings. Finally, the detected results were compared with the observation data of GPS ground control stations.

I. INTRODUCTION

The Mw9.0 Tohoku Earthquake occurred on March 11, 2011, off the Pacific coast of the northeastern (Tohoku) Japan, caused gigantic tsunamis, resulting in widespread devastation. It also caused large crustal movements over a wide area. Due to this event, Japan had experienced over 900 aftershocks and induced events by September 7, 2012, with about 60 being over magnitude 6.0 and three over magnitude 7.0. The Fukushima Earthquake with Mw7.1 occurred on April 11, 2011 was one of the most damaging induced earthquakes. The epicenter was located at 37.01º N, 140.48º E. It also caused numerous fault scarps, with a maximum displacement of 2.3 m. This earthquake occurred in the vicinity of the Idosawa Fault, which is a shallow crustal fault near Tabito, Iwaki City, Fukushima Prefecture. The vertical displacements from 0.8 m to 1.5 m have been observed by ground surveys.

Two methods have normally been used to detect crustal movements from remote sensing images in the past studies. The first one is differential interferometric analysis of synthetic aperture radar (DInSAR) [2-3]. The second one is the pixel-offset method, which can be applied to both SAR and optical images [4-5]. In the 2011 Tohoku earthquake, the extent of crustal movements was much larger than SAR imaging areas. Due to the absence of the accurate geocoding information, it was difficult to detect the absolute displacement using the previous methods. The high-accuracy georeferenced product, however, has become available recently due to the improvement of SAR sensors and thus an improved pixel-offset method was proposed by the present authors to estimate the absolute ground displacements even in the case of large-scale tectonic movements [6]. In our previous research, the proposed method has been tested on 4 temporal TerraSAR-X (TSX) images along the Sendai coast and the result was found to be highly accurate through the comparison with GPS recordings.

In this study, two pairs of pre- and post-event SAR images were used to detected crustal movements by the DInSAR analysis and our pixel-offset method, respectively. The results from the two methods and the different SAR data sets were compared and discussed. The accuracy was demonstrated by comparing the detected displacements with those from the GPS ground station records.

II. STUDY AREA AND IMAGE DATA

The study area was focused on the coastal zone of Fukushima Prefecture as shown in Fig. 1. The pre-event ALOS/PALSAR image was taken on March 3, 2011 while the post-event one was taken on April 18, 2011. Since the pre-event image was taken before the main shock, the detected crustal movements from this pair include the influence of the main shock. The two images were taken in the ascending path by the Fine Beam Single Polarization (FBS) mode, with the 6.25 m resolution in both the azimuth and range directions. The PALSAR images were provided as Single Look Complex (SLC) products.

The pre-event TSX image was taken on March 14, 2011 while the post-event one on September 5, 2011. Since the both images were taken after the main shock, the crustal movements caused by the event were not included in the result from this pair. The two images were in the descending path. Since the images were acquired in the StripMap mode, the original resolutions were 3.30 m in the azimuth and 1.94 m in the range directions, respectively. The TSX data were provided as Single-Look Slant-Range Complex (SSC) products. However, the proposed pixel-offset method needs the geo-coded orthorectified intensity images. The EEC products processed by DLR were also used in this study. Both the PALSAR and TSX images were captured with HH polarization.

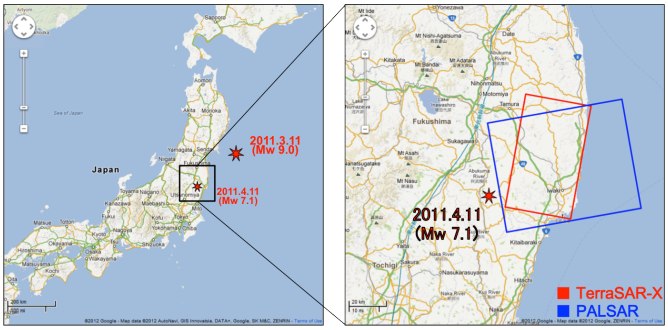

Fig.1 Study area along the Pacific coast of Fukushima Prefecture.

III. Interferometric Analysis

A DInSAR analysis was applied to the SLC products of the PALSAR images using *SARscape* software to detect the crustal movement. Firstly, an initial InSAR result was obtained using the two complex imagery data. Then a 30 m resolution ASTER Global Digital Elevation Model (ASTER GDEM) was introduced to remove elevation effects from the initial result. Orbital fringes and noises were removed by the Goldstein filter. Finally, the geocoded coherence and final differential interferogram were obtained. The obtained coherence and interferogram are shown in Fig. 2. The spatial normal baseline length is 483 m while the temporal baseline is 46 days. Due to the L-band wavelength and the short time lag, most of the target area shows coherence values higher than 0.5. Thus, the fringes in the interferogram were consecutive in the whole target area. From the interferogram, it could be confirmed that the target area moved to the east direction after the main shock, away from the PALSAR sensor in the ascending path. However, localized significant displacements were confirmed around the Yunotake, Shinohara and Idosawa faults, where surface raptures were observed by the 11 April 2011 Fukushima earthquake.

The DInSAR analysis was also applied to the SSC products of TSX, whose spatial normal baseline length is 104 m while the temporal baseline is 176 days. The coherence in the ground range was obtained and shown in Fig. 3(b). Due to the short wavelength of X-band SAR, the coherence in forest areas is very low. Since more than half of the target area was mountainous covered by vegetation, DInSAR fringes could not be detected in these areas. In addition, the 6-month time lag between the two images also caused low coherence. As a result, the average value of the coherence for the two TSX images was about 0.25. Only parts of the urban area along the coastline show high coherence larger than 0.5. The interferogram in the high coherence area is highlighted in Fig. 3(b). From the interferogram, it could be confirmed that the urban area moved to the east direction, close to the TSX sensor in the descending path, which is similar trend to the result from the PALSAR data. Comparing these results by the two SAR sensors, it was recognized that although the X-band can detect minor movements from 1.6 cm, the L-band shows higher capability in the DInSAR analysis.

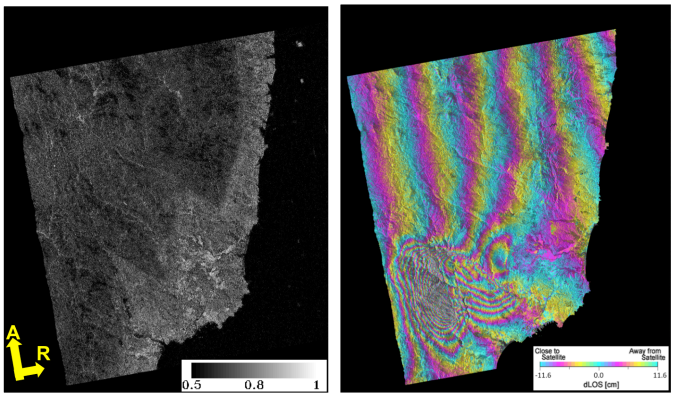

(a) (b)

Fig. 2 Coherence (a) and interferogram (b) obtained from the pre- and post-event PALSAR data pair.

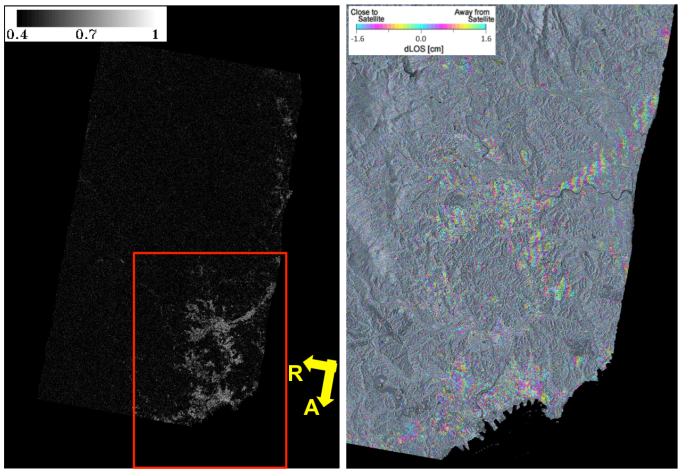

(a) (b)

Fig. 3 Coherence (a) and the part of interferogram (b) within the red frame in (a), obtained from the pre- and post-event TerraSAR-X data pair.

IV. Pixel Offset Method

Since the accuracy of pixel-offset methods depends on the spatial resolution of SAR images, it is difficult to detect the 1 m movements from PALSAR images with 6 m resolution. Thus, the pixel-offset method was applied only to the TSX images with 3 m resolution. The digital number of the TSX's EEC products was transformed to a sigma naught (σ^0) value firstly. To minimize any loss of information included in the intensity images, the window size of the Lee filter was set as 3 × 3 pixels. Since the orbit type of our TSX images was "Science", their required orbit accuracy is within 20 cm, but actual data showed better than 10 cm accuracy [7]. The color composite of the two temporal TSX intensity images after the pre-processing is shown in Fig. 4(a).

The crustal movements within the red frame in Fig. 4(a) were extracted by the proposed pixel-offset method [6]. Firstly, the whole target area was divided into a 2.5 × 2.5 km^2 mesh. In each sub-area (2.5 × 2.5 km^2), solid buildings larger than 150 m^2 were extracted by simple segmentation. The threshold

value of the backscattering intensity used in segmentation was set as -2.5 dB, which means the pixels whose σ_0 values are larger than -2.5 dB were grouped as a building object. Then the non-changed buildings were extracted by comparing the building locations in the two building images. The displacement of a non-changed building between the two TSX intensity images was calculated by an area correlation method. To improve the accuracy, parts of the TSX images around non-changed buildings were resampled to 0.25 m/pixel by cubic convolution to have 1/5 of the original pixel size. Thus, the shift of building shapes could be detected at a sub-pixel level. When the correlation coefficient of a non-changed building in the two TSX image was larger than 0.8, the detected displacement was counted as valid data. Finally, the average value of these movements was calculated and considered as the crustal movement in that sub-area.

The crustal movements in the whole area were detected in the same way. To ensure the reliability of the results, only a sub-area containing more than 5 building displacements was counted as valid one. Since the displacements were calculated from the location of buildings, the proposed method could not be applied to mountainous areas without buildings. The movements from 127 sub-areas were detected, and they are shown in Fig. 4(b). The displacements of four sub-areas including GPS stations were detected. Two sub-areas including Fukushima-kawauchi and Iwaki-4 GPS stations could not be detected due to the small number of buildings. The detected crustal movements in the four GPS sub-areas and the movements in neighboring sub-areas for the two GPS stations were shown in Table I. A comparison of the detected movements in the table shows that the largest movement occurred around the Iwaki-2 GPS station. The westward movement, the opposite direction with the other areas, was detected around the Iwaki-4 station, located on the southwest side of Shinonohira fault.

The displacement amplitude is shown in Fig. 5(a) by the rainbow color. The largest detected movement was 1.23 m of which 1.1 m to the east and 0.23 m to the north directions. The number of buildings' displacements detected in each sub-area is shown in Fig. 5(b). More number the detected buildings' displacements were, more reliable the obtained result became. It was confirmed that several crustal movements that were directed to different directions with the surrounding sub-areas in Fig. 4(b) were those with small numbers of detected displacements in Fig. 5(b). However, the detect result became stable when the number of buildings' displacements were more than 10.

V. Verification of Detected Results

To verify the accuracy of the detected movements by the two methods, the crustal movement data from the GPS stations were introduced. The surface displacement is a vector in the three-dimensional (3D) space with three components, D_E, D_N, and D_Z, to the east, north, and vertical directions, respectively.

The result of DInSAR analysis can only detect the movement to the slant range. The 3D movements (D) can be converted to the movement to the range direction (M_S) by the following relationship.

$$M_S = (D_E \cos\alpha - D_N \sin\alpha)\sin\theta + D_Z \cos\theta \quad (1)$$

where D is the actual movement to the east, north, and vertical directions; M is the shift in the SAR image; α is the heading angle clockwise from the north; and θ is the radar incidence angle.

It should be noted that DInSAR could only provide the relative displacement within the target area. Thus, the GPS Takine station was set as the reference, and the displacements between the Takine and other stations were calculated. The *Ms* was obtained from the unwrapped image as shown in Table I. The GPS recordings obtained at 6 sites between March 3 and April 18, 2011 were converted using (1) as shown in Table I. The displacement corresponding to one fringe in the interferogram is half of the wavelength, which is 11.6 cm. The

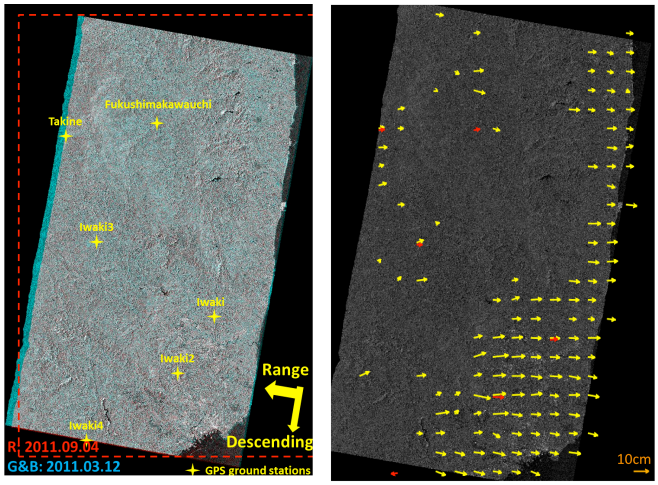

(a) (b)

Fig. 4 Color composite of the pre- and post-event TSX images (a); and detected displacement vectors in each sub-area overlapping on the pre-event TSX intensity image (b), compared with the GPS observed record shown in red arrows.

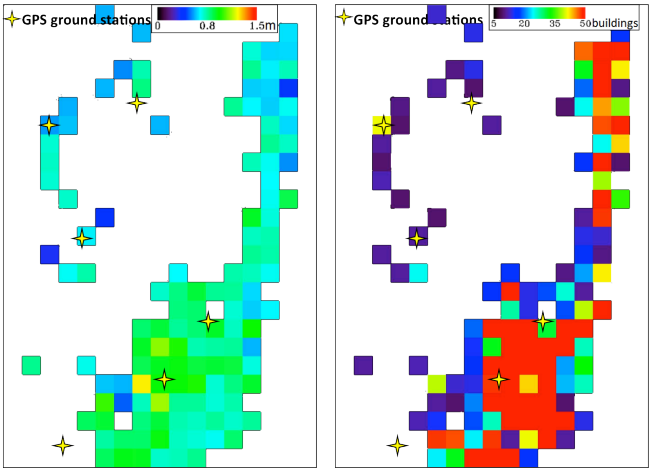

(a) (b)

Fig. 5 Displacement amplitude shown in the rainbow color (a); and the number of building displacements used in each sub-area (b).

TABLE I COMPARISON OF DETECTED CRUSTAL MOVEMENTS AROUND THE GPS STATIONS BY THE DINSAR ANALYSIS FROM PALSAR DATA AND THE PROPOSED METHOD FROM TSX IMAGES, WITH THE GPS RECORDS (UNIT: METER).

GPS stations	DInSAR (away) [March 3 to April 18]			Pixle-offset [March 13 to Sep. 4]			
	PALSAR	GPS	Errors		TSX	GPS	Errors
Fukushima-kawauchi	0.36	0.21	0.15	E	0.46	0.41	0.05
				N	0.14	-0.08	0.22
Takine	Reference	Reference	-	E	0.38	0.4	-0.02
				N	-0.08	-0.06	-0.02
Iwaki-3	0.05	0.03	0.02	E	0.46	0.38	0.08
				N	-0.18	-0.01	-0.17
Iwaki	0.64	0.30	0.34	E	0.66	0.52	0.14
				N	0.04	-0.07	0.11
Iwaki-2	0.50	0.27	0.23	E	0.87	0.74	0.13
				N	-0.09	-0.02	-0.07
Iwaki-4	0.73	0.31	0.42	E	-0.29	-0.43	0.14
				N	0.07	0.3	-0.23

averaged differences between the DInSAR result and GPS measurement were about 0.23 m to the north, with the maximum difference was 0.42 m. The errors were caused by the orbit precision. Since the whole target area moved due to the main shock, it was difficult to assign the reference point. Thus, the orbit errors still left in our results.

The proposed pixel-offset method can detect a 2D movement from TSX intensity images to the east and north directions. The movement in the vertical direction is decomposed and transformed into the movements to the east and north directions. The relationship between an actual crustal movement and its 2D shift in a ground range SAR image is shown in (2).

$$\begin{pmatrix} M_E \\ M_N \end{pmatrix} = \begin{pmatrix} 1 & 0 & -\cos\alpha / \tan\theta \\ 0 & 1 & \sin\alpha / \tan\theta \end{pmatrix} \begin{pmatrix} D_E \\ D_N \\ D_Z \end{pmatrix} \quad (2)$$

where M_E and M_N are the shift in the SAR image to the east and north directions, respectively.

The displacements between March 13 and September 5, 2011 converted from the GPS records were calculated by (2), and shown in Table I. The converted GPS displacements are also shown in Fig. 4(b) by red arrows. A comparison of the results detected around the GPS stations with the converted GPS recordings demonstrated a very high level of consistency. The averaged differences between the detected result and the GPS measurement were about 0.10 m to the east and 0.14 m to the north. The maximum difference was 0.27 m. Comparing with the DInSAR results, the proposed pixel-offset method could show higher accuracy.

VI. CONCLUSIONS

In this study, we applied a DInSAR analysis and an improved pixel-offset method for detecting crustal movements due to the 11 April 2011 Fukushima Earthquake from two temporal PALSAR and TerraSAR-X data. The crustal movements were estimated from these two methods. Due to the long wavelength of the L-band SAR and the short time lag between the two PALSAR data, the interferogram was obtained in the whole target area. However, the interferogram was obtained only for a part of the urban area from TSX due to decorrelation.

Since the proposed pixel-offset method focused on non-changed buildings, it works only in the area including buildings. However, the proposed method can detect the absolute two-dimensional displacement, more information than a one-directional (slant-range) DInSAR analysis. The records at six GPS ground stations were introduced to verify the accuracy of our detection. The DInSAR result from the PALSAR data and the one from the pixel-offset method from the TSX images show similar accuracy, around 0.3 m. It could be confirmed that the DInSAR result can grasp the trend for the whole area easily while the pixel-offset method can overcome decorrelation caused by vegetation and a long time-lag acquisition.

ACKNOWLEDGMENT

PALSAR data was owned by the Japan Aerospace Exploration Agency (JAXA). TerraSAR-X data was owned by German Aerospace Center (DLR) and provided by PASCO Corporation.

REFERENCES

[1] K.I. Kelson, L.F. Harder, T, Kishida, and I. Ryder, "Preliminary observations of surface fault rupture from the April 11, 2011 Mw6.6 Hamadoori Earthquake, Japan," Geotechnical Extreme Events Reconnaissance, No. GEER-025d, 2011.

[2] S.F. Stramondo, R. Cinti, M. Dragoni, S. Salvi, and S. Santini, "The August 17, 1999 Izmit, Turkey, earthquake: Slip distribution from dislocation modeling of DInSAR and surface offset," Annals of Geophysics, vol. 45, No. 3/4, pp. 527-536, 2002.

[3] M. Chini, S. Atzori, E. Trasatti, C. Bignami, C. Kyriakopoulos, C. Tolomei, and S. Stramondo, "The May 12, 2008, (Mw 7.9) Sichuan Earthquake (China): Multiframe ALOS-PALSAR DInSAR Analysis of Coseismic Deformation," IEEE Geoscience and Remote Sensing Letters, vol. 7, No. 2, pp. 266-270, 2010.

[4] M. Tobita, H. Suito, T. Imakiire, M. Kato, S. Fujiwara, and M. Murakami, "Outline of vertical displacement of the 2004 and 2005 Sumatra earthquakes revealed by satellite radar imagery," Earth Planets Space, vol. 48, No. 1, pp. e1-e4, 2006.

[5] P.J. González, M. Chini, S. Stramondo, and J. Fernández, "Coseismic horizontal offsets and fault-trace mapping using phase correlation of IRS satellite images: The 1999 Izmit (Turkey) Earthquake," IEEE Trans. on Geos. Remote Sensing, vol. 48, No. 5, pp. 2242-2250, 2010.

[6] W. Liu, and F. Yamazaki, "Detection of crustal movement from TerraSAR-X intensity images," IEEE Geoscience and Remote Sensing Letters, vol. 10, No. 1, pp. 199-203, 2013.

[7] M. Wermuth, A. Hauschild, O. Montenbruck, and A. Jäggi, "TerraSAR-X Rapid and Precise Orbit Determination," In: 21st International Symposium on Space Flight Dynamics, France, 2009.